Dalton Transactions

ROYAL SOCIETY OF CHEMISTRY

PAPER

View Article Online
View Journal | View Issue

Cite this: *Dalton Trans.*, 2025, **54**, 17646

Organoruthenium(II) complexes with adamantane-thiourea ligands: structural and biological insights

Chi-Xin Guo, †[a] Rahime Eshaghi Malekshah, †[a] Tzu-Yu Chen, [b,c] Amir Karim, [a] Yu-Ting Chu, [d] En-De Shu, [e] Chien-Chih Chiu,[e] Ching-Ming Chien *[c] and Sodio C. N. Hsu *[a,f]

Received 17th August 2025,
Accepted 7th October 2025

DOI: 10.1039/d5dt01959a

rsc.li/dalton

Organometallic ruthenium complexes have gained significant attention as promising anticancer agents due to their favorable properties in medicinal chemistry. In this study, four adamantane-*N*-acylthiourea-based ligands (**ADL1–ADL4**) and their corresponding Ru(η^6-*p*-cymene) complexes (**RuAD1–RuAD4**) were synthesized and characterized using $^{13}C\{^1H\}$ NMR, FT-IR, UV–vis spectroscopy, and ESI (HR)-MS. Additionally, the structures of all complexes were confirmed through single-crystal X-ray diffraction analysis. The *in vitro* cytotoxicity of the compounds was evaluated against human melanoma (A375), triple-negative breast cancer (MDA-MB-231), and colon cancer (HCT116 and SW620) cell lines, resulting in the selection of **RuAD1** for further studies due to its superior anticancer activity. Further investigations on A375 cells showed that adamantane–ruthenium complexes exhibited stronger cytotoxicity than their corresponding ligands and other cell lines, leading to pronounced morphological alterations, inhibition of migration, and induction of apoptosis. Western blot analysis indicated that these effects were likely mediated through activation of intrinsic, mitochondrial-dependent apoptotic pathways. Additionally, *in silico* ADMET analysis supported the biological findings, identifying **RuAD1** as having the most favorable pharmacokinetic profile among the tested compounds.

Introduction

Organometallic half-sandwich Ru(II) complexes have emerged as highly promising candidates in anticancer drug development, thanks to their unique structural versatility and potent biological activities.[1–4] Ruthenium(II)–arene RAPTA-type compounds have garnered significant interest due to their extensively studied therapeutic potential.[5] By modifying the functional groups on the ligands, researchers can fine-tune the reactivity of these complexes, directly influencing their chemical stability and biological activity. This ability to modify ligands has made the Ru(II)–arene system a focal point in drug design.

The ligands within this system play a crucial role in determining the anticancer efficacy of the complexes. *N*-Acylthiourea ligands, for example, are well-known for their wide array of biological activities and robust air- and moisture-stability.[6,7] Featuring oxygen, nitrogen, and sulfur donor atoms, these ligands enable versatile coordination with metal centers, which in turn enhances the biological and pharmacological properties of the resulting complexes.[8,9] The inclusion of thiourea groups further boosts biological activity, contributing to metal coordination and hydrogen bonding, key mechanisms in anticancer action.[10]

Adamantane derivatives, initially developed as antiviral[11–13] and anticancer[14,15] agents, also hold significant therapeutic value in other medical areas.[16,17] Amantadine and rimantadine were among the first to target influenza strains,[18–20] while derivatives like memantine have proven effective in treating neurological disorders such as Parkinson's disease.[21] Several clinically approved drugs are derived from the adamantane

[a]*Department of Medicinal and Applied Chemistry, Drug Development and Value Creation Research Centre, Kaohsiung Medical University, Kaohsiung 807378, Taiwan. E-mail: sodiohsu@kmu.edu.tw*
[b]*Department of Life Sciences, National Central University, Taoyuan, 320317, Taiwan*
[c]*Department of Applied Chemistry, National Chiayi University, Chiayi, 600355, Taiwan. E-mail: cmchien@mail.ncyu.edu.tw*
[d]*International PhD Program for Science, National Sun Yat-Sen University, Kaohsiung 804201, Taiwan*
[e]*Department of Biotechnology, Kaohsiung Medical University, Kaohsiung 807378, Taiwan*
[f]*Department of Medical Research, Kaohsiung Medical University Hospital, Kaohsiung 807378, Taiwan*
†These authors contributed equally to this work.

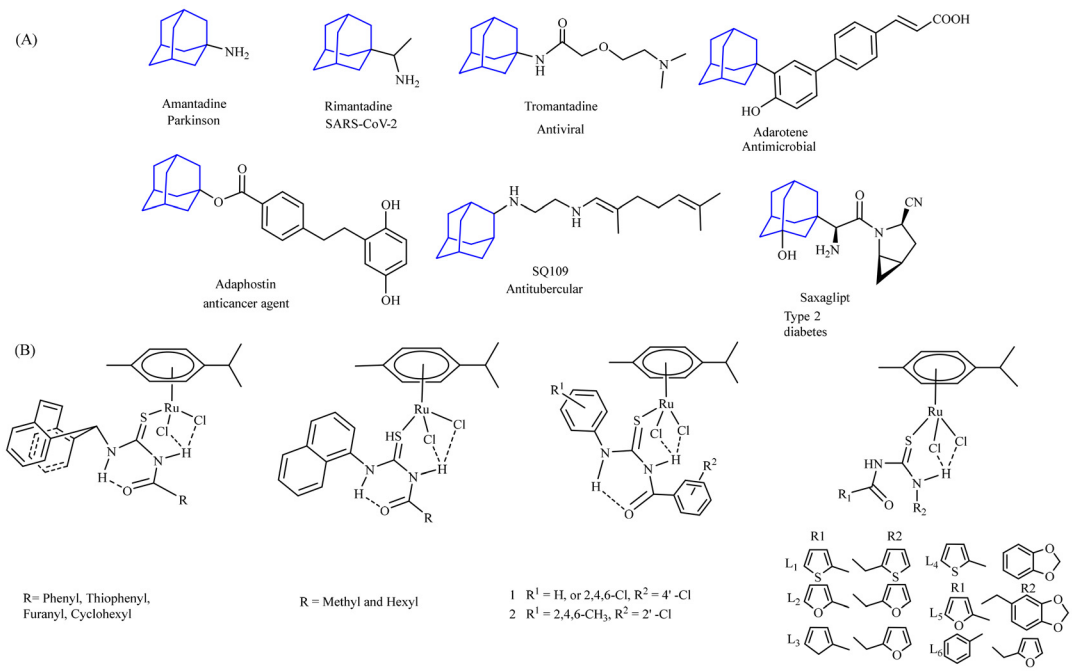

Scheme 1 (A) Representative adamantane-derived compounds and their structural frameworks.[17] (B) Ru(II)-based *N*-acylthiourea complexes synthesized as potential anticancer agents.[22–25]

scaffold (Scheme 1A). Although Ru(II)-based *N*-acylthiourea anticancer agents have not yet received clinical approval, they have been extensively investigated, as illustrated in Scheme 1B. The adamantane moiety, with its rigid, cage-like structure, contributes significantly to the stability and solubility of the drug complexes. This stability enhances their therapeutic potential in drug design. In this study, we report the synthesis of four new adamantane-thiourea ligands and their corresponding Ru(II)–arene complexes, which have demonstrated considerable cytotoxic effects against cancer cell lines (A365, MDA-MB-231, HCT116, and SW620), underscoring their potential in cancer treatment.

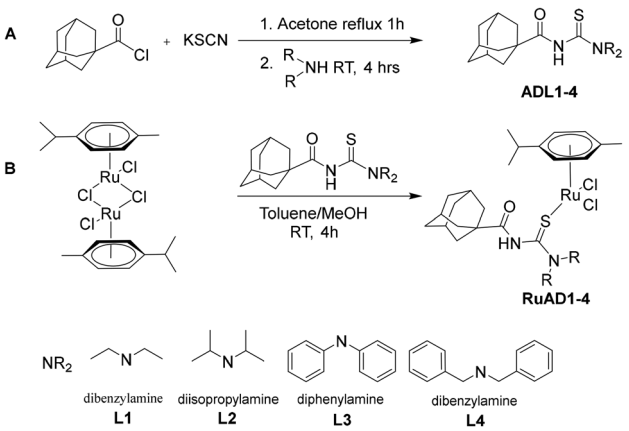

Scheme 2 Illustration of the synthesis of the adamantane-1-carboxamide-based ligands (**ADL1–ADL4**) (A) and their complexes **RuAD1–RuAD4** (B).

Result & discussion

Synthesis and characterization of ligands and organoruthenium(II) complexes

The adamantane-1-carboxamide-based ligands (**ADL1–ADL4**) were synthesized in two stages. First, 1-adamantanecarbonyl chloride was reacted with a slight excess of potassium thiocyanate. In the second stage, the corresponding amines (diethylamine (**L1**), diisopropylamine (**L2**), diphenylamine (**L3**), and dibenzylamine (**L4**)) were added to complete the reactions (Scheme 2A). To synthesize complexes **RuAD1–RuAD4**, a solution of $[RuCl_2(\eta^6\text{-}p\text{-cymene})]_2$ in toluene was added to solutions of corresponding adamantane-thiourea ligands (**ADL1–ADL4**) to give precipitates (Scheme 2B). The synthesized ligands and complexes were characterized by FT-IR, UV–vis, ^{1}H and ^{13}C NMR spectroscopy and high-resolution ESI mass spectrometry, and detailed results are presented in Fig. S1–S42 of the SI.

The UV–vis spectra of the **ADL1–ADL4** ligands exhibited bands at 203–254 and 279–309 nm, corresponding to characteristic $\pi \rightarrow \pi^*$ (aromatic rings as well as C=O and C=S groups) and $n \rightarrow \pi^*$, respectively.[26] Furthermore, $n \rightarrow \pi^*$ and $\pi \rightarrow \pi^*$ intra-ligand transition bands and MLCT metal to ligand charge transfer bands of these complexes were observed at 257–327 nm. Additionally, the less intense band observed at 427–434 nm in the spectra of Ru(II) complexes corresponds to $d \rightarrow d$ transitions.[22,27] UV–vis spectra of the ligands and complexes are presented in Fig. S1 and S2, respectively. FT-IR spectra of the **ADL1–ADL4** ligands exhibited a characteristic

C═S stretching frequency in the range of 1195–1235 cm^{-1} (Fig. S3–S6).[28] In the corresponding **RuAD1–RuAD4** complexes (Fig. S7–S10), this frequency shifted to 1191–1209 cm^{-1}, indicating a reduction in the double bond character of the C═S bond.[29–32] The carbonyl stretching frequency of the free ligands (1642–1709 cm^{-1})[33] increased to 1697–1715 cm^{-1} upon complexation. This was further supported by the shift in the N–H stretching frequency from 3276–3341 cm^{-1} in the free ligands to 3110–3139 cm^{-1} in the complexes.[34]

In the ^{1}H NMR spectra of **ADL1–ADL4** in $CDCl_3$ (Fig. S11–S14), the N–H proton associated with the thiocarbonyl group appeared as a singlet at 7.65, 7.39, 8.11, and 7.96 ppm, respectively. Upon monodentate coordination with ruthenium in **RuAD1–RuAD4** (Fig. S15–S18), these signals shifted downfield to 10.01, 9.84, 10.73, and 10.57 ppm, respectively. This notable downfield shift indicated coordination of the ligand to the metal center *via* the sulfur atom of the thiocarbonyl group. The broad signals of the methylene group (N–CH_{2b}) in **ADL1** is 3.95 and 3.45 ppm,[30] which shifted to 4.05–4.02 and 3.34–3.29 ppm in the **RuAD1** complex. Furthermore, **ADL2** exhibited a single broad signal between 1.64 and 1.11 ppm, attributed to the (CH_{3c})$_2$ groups of the adamantane ligand, which shifted to the range around 1.47 ppm in the **RuAD2** complex. For **ADL4**, the broad N–CH_{2b} signals initially observed at 5.15 and 4.57 ppm were slightly shielded in **RuAD4**, appearing at 4.40 and 5.03 ppm. **RuAD1–RuAD4** complexes exhibited two doublets in the range of 5.45–5.36 and 5.20–5.17 ppm,[35] corresponding to the aromatic protons of the π-coordinated *p*-cymene ligand. Singlet peaks observed at 2.23, 2.24, 2.20, and 2.13 ppm in **RuAD1–RuAD4** were assigned to the methyl protons of *p*-cymene. Additionally, heptet signals appearing between 3.03 and 2.63 ppm in **RuAD1–RuAD4** were attributed to the CH proton of the isopropyl group within the *p*-cymene moiety. ^{1}H NMR spectra of **RuAD1–RuAD4** recorded in DMSO-d_6 are shown in Fig. S19–S22.

The ^{13}C NMR spectra of **ADL1–ADL4** in $CDCl_3$ displayed characteristic signals for C═S and C═O carbons in the ranges of 183.21–178.97 ppm and 174.86–172.36 ppm, respectively (Fig. S23–S26). Upon coordination with ruthenium to form **RuAD1–RuAD4** (Fig. S27–S30), these peaks shifted to higher chemical shifts, indicating interaction between the metal center and the ligand donor atoms.[25] The ^{13}C NMR spectra of the adamantane moiety in the **RuAD1–RuAD4** complexes exhibited no significant chemical shift changes compared to the corresponding ligands. Signals at 30.76 ppm for **RuAD1**, 30.96 ppm for **RuAD2**, 30.67 ppm for **RuAD3**, and 30.65 ppm for **RuAD4** were attributed to the CH proton of the propyl group of *p*-cymene. Additionally, the ESI-HRMS of **ADL1–ADL4**, recorded in positive electrospray ionization mode in the presence of trace Na^+, confirmed the expected molecular masses, as shown in Fig. S31–S34. The formation of $[L + H]^+$, $[L + Na]^+$, and $[2L + Na]^+$ ion peaks is likely attributed to intramolecular rearrangements.[36] For **RuAD1–RuAD4**, HRMS displayed prominent peaks at *m*/*z* 529.1819, 557.2132, 625.1817, and 653.2132, respectively, corresponding to the fragment ions $[M\text{-}HCl\text{-}Cl^-]^+$ (Fig. S35–S38).[30]

Molecular structures and coordination behavior of acylthiourea ligands

Single crystals of **RuAD1–RuAD4**, suitable for X-ray diffraction analysis, were obtained by the slow evaporation of a methanol/diethyl ether solution, yielding orange crystals for all four complexes. The X-ray crystallographic results of **RuAD1–RuAD4** are illustrated in Fig. 1, and key bond distances and angles are listed in Table S2. Each complex exhibited a half-sandwich three-legged piano-stool geometry configuration, wherein the Ru(II) center is coordinated by two chlorido ligands and a sulfur atom from the acylthiourea ligand, forming the legs, while the six carbon atoms of the η^6-*p*-cymene ligand constitute the seat. The complexes crystallized in distinct crystal systems: **RuAD1** ($P21/c$) and **RuAD3** ($P21/n$) in the monoclinic crystal system; **RuAD4** ($P\bar{1}$) in the triclinic, centrosymmetric space group; and **RuAD2** ($R\bar{3}$) in the trigonal system. The Ru(1)–S(1) bond lengths for the **RuAD1–RuAD4** complexes are 2.4045(6), 2.3889(4), 2.3934(13) and 2.4074(10) Å, respectively, aligning with previously reported values for C═S double bonds in analogous Ru(II) acylthiourea complexes, reflecting the monodentate coordination mode *via* the thiocarbonyl sulfur.[37,38] Intriguingly, the crystal structures reveal an intramolecular hydrogen bond between the N1–H hydrogen and a neighboring chlorido ligand coordinated to Ru(II), which elongates the affected Ru(II)–Cl bond relative to other Ru(II)–Cl bonds in the coordination sphere. The bond angles, S(1)–Ru(1)–Cl(1), S(1)–Ru(1)–Cl(2), and Cl(1)–Ru(1)–Cl(2) span 90.74(2)°–88.13(5)°, 88.348(19)°–93.25(5)°, and 87.79(4)°–91.612(19)°, respectively, consistent with the distorted octahedral geometry typical of piano-stool complexes.

The coordination behavior of acylthiourea ligands was found to be strongly influenced by their structural features, particularly the nature of the thioamide moiety. Deprotonation at the amide nitrogen typically promotes bidentate coordination, leading to the formation of either SN- or SO-type chelates. In general, ligands incorporating a primary thioamide moiety favor SN bidentate coordination,[39,40] whereas those containing a secondary thioamide moiety predominantly form SO bidentate complexes.[25] Notably, monodentate coordination appears to be independent of the primary or secondary nature of the thioamide group. Our observations indicate that ligands with primary thioamide functionalities can coordinate in a monodentate fashion through the thiocarbonyl sulfur atom.[41,42] However, to the best of our knowledge, there have been no prior reports of secondary thioamide-based acylthiourea ligands forming monodentate neutral complexes. The present work provides the first evidence of such ligands coordinating monodentately to a Ru(II) center in Ru(II) *p*-cymene complexes, expanding the coordination versatility of acylthioureas. This unprecedented coordination mode expands the known binding versatility of acylthiourea ligands and highlights the subtle influence of ligand design on metal–ligand interactions.

In silico ADMET prediction analysis for absorption and blood–brain barrier permeability

The pharmacokinetic characteristics of the synthesized Ru–adamantane derivatives were evaluated by *in silico* ADMET

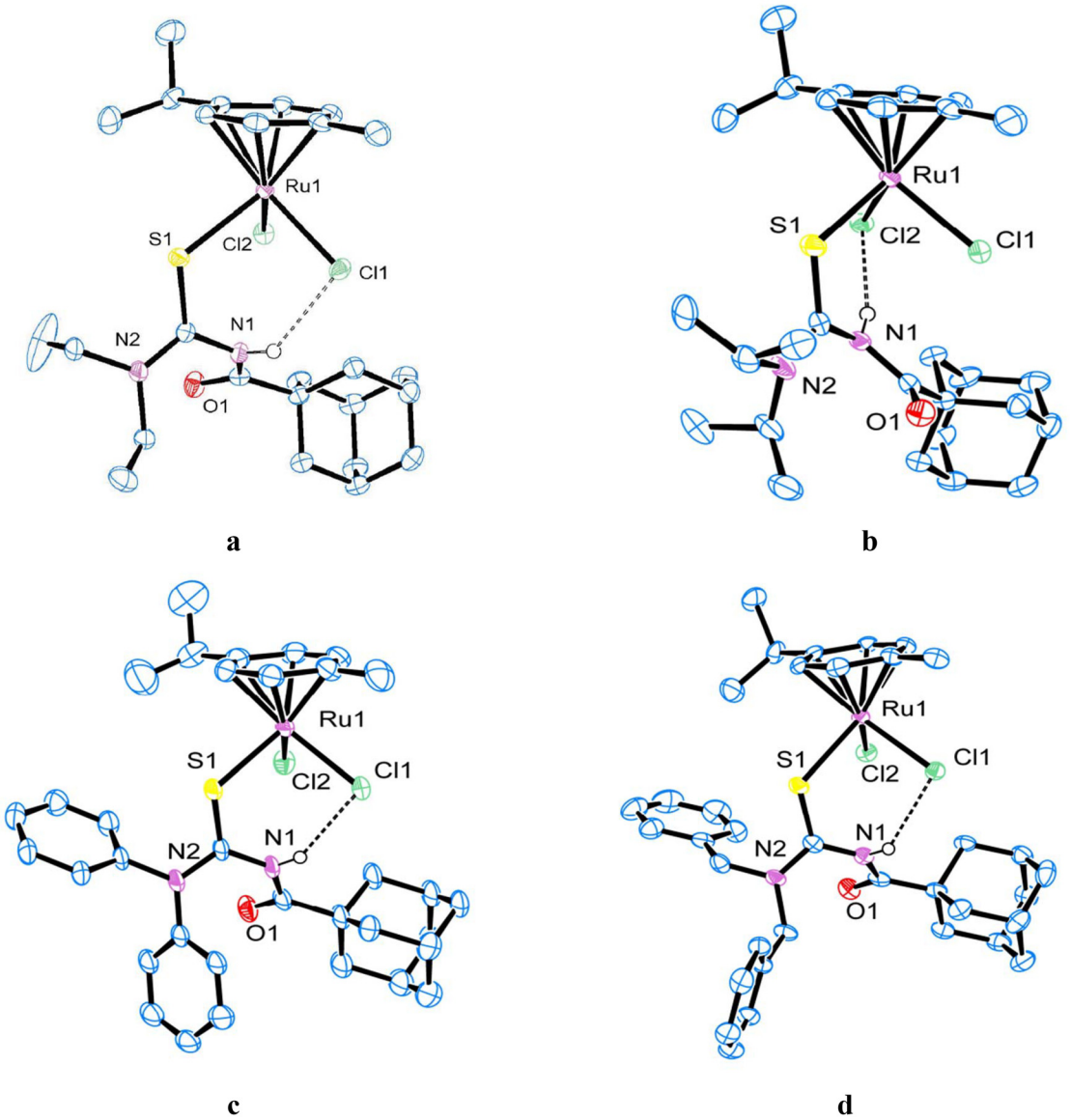

Fig. 1 Thermal ellipsoidal plots of (a) **RuAD1**, (b) **RuAD2**, (c) **RuAD3**, and (d) **RuAD4** at the 50% probability level, with hydrogen atoms omitted for clarity.

(absorption, distribution, metabolism, excretion, and toxicity) using Discovery Studio 2022. As shown in Fig. 2 and S39 and summarized in Table 1, **RuAD1** and **RuAD2** were predicted to penetrate the blood–brain barrier (BBB permeability), whereas **RuAD3** and **RuAD4** were not. The lack of BBB penetration for **RuAD4** may be attributed to its relatively large polar surface area (PSA), which can hinder passive diffusion across lipid membranes. Based on the absorption classification in Fig. 2, **RuAD1**, **RuAD2**, and **RuAD3** were located within the high-absorption region (Absorption-95 ellipse), whereas **RuAD4** was outside this region, indicating low predicted absorption. Notably, **RuAD1** was classified as High in liver absorption score (LAS), with >90% plasma protein binding (PPB) and predicted as a non-inhibitor of CYP2D6. Collectively, these results indicate that **RuAD1** possesses the most favorable ADMET profile among the tested compounds, characterized by high absorption potential, strong plasma protein binding, absence of CYP inhibition, moderate BBB permeability, and favorable liver absorption properties for oral administration.

In vitro cytotoxicity evaluation of adamantane-thiourea ligands and ruthenium complexes

The antiproliferative activity of the adamantane-thiourea ligands (**ADL1–ADL4**) and complexes (**RuAD1–RuAD4**) was investigated against human melanoma A375 cells, triple negative breast cancer MDA-MB-231 cells, and colon cancer HCT116 and SW620 cells by MTS (3-(4,5-dimethylthiazol-2-yl)-5-(3-carboxymethoxyphenyl)-2-(4-sulfophenyl)-2*H*-tetrazolium)

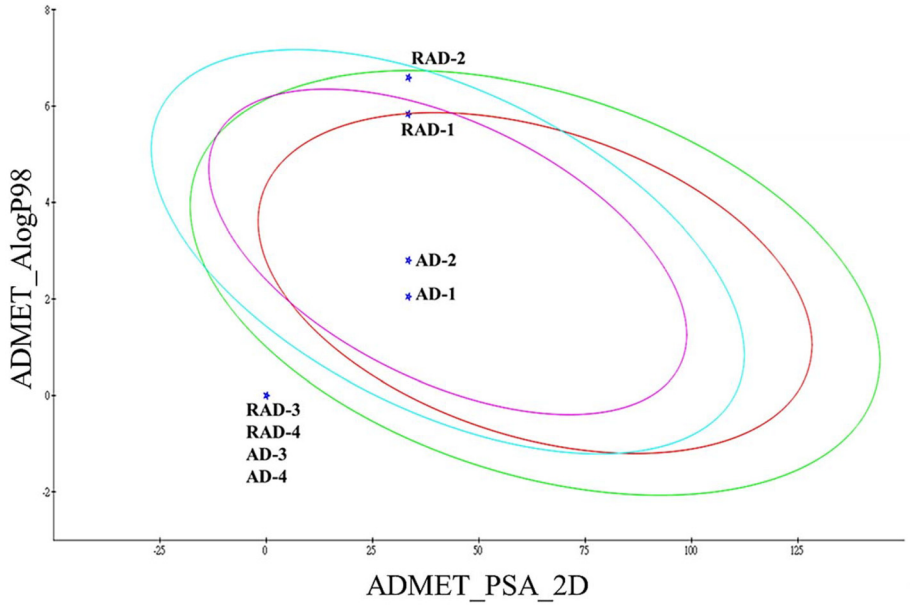

Fig. 2 2D ADMET profile for the **ADL1–ADL4** ligands and **RuAD1–RuAD4** complexes.

Table 1 ADMET screening for the ligands and complexes

Compound	BBB	LAS	LIA	CYP enzyme inhibitor	LPPB (%)
ADL1	High	High	Good	No inhibition	>90
ADL2	High	High	Good	No inhibition	>90
ADL3	Low	Low	Bad	CYP2D6	<90
ADL4	Low	High	Bad	CYP2D6	<90
RuAD1	High	High	Good	No inhibition	>90
RuAD2	High	Low	Good	No inhibition	<90
RuAD3	Low	High	Good	No inhibition	>90
RuAD4	Low	Low	Bad	CYP2C9	<90

BBB (blood–brain barrier), LAS (liver absorption score), LIA (liver inhibition activity), LPPB (lipid plasma protein binding).

assay for 48 h (Fig. 3A–D). The IC_{50} values for *in vitro* cytotoxicity are listed in Table 2. Among these cell lines, A375 cells showed the highest sensitivity when compared to other cell lines. In contrast, the HCT116 cell line showed the lowest sensitivity. In addition, among the ligands, compounds **ADL2** and **ADL4** revealed the highest cytotoxicity in A375 cells, with an IC_{50} values of 18.5 ± 2.6 μM and 19.1 ± 1.2 μM, respectively. Furthermore, all ruthenium complexes (**RuAD1–RuAD4**) revealed enhanced cytotoxicity in comparison with their respective ligands (**ADL1–ADL4**), with **RuAD1** showing the most significant cytotoxic effect on A375 melanoma cells (IC_{50} = 9.3 ± 1.2 μM). Moreover, the cytotoxicity of **RuAD1** at 5, 10, and 20 μM concentrations revealed selective cytotoxicity towards cancer and normal cells. As shown in Fig. 3E, the cell viability of normal human M10 cells exposed to **RuAD1** (5, 10, and 20 μM) for 48 h was 99.5%, 92.7%, and 82.5%, respectively. Under identical conditions, cell viabilities of A375 cells reached 98.2%, 85.3%, and 23.5%, respectively. These results indicated that **RuAD1** exhibited selective cytotoxicity towards cancer cell lines with reduced toxicity toward normal cells. Arunachalam *et al.* synthesized binuclear Ru(II) complexes with N^O and N^S chelation (**1–3**) and tested their activity against breast (MCF-7), colon (HT-29), and liver (HepG2) cancer cell lines, along with noncancerous kidney (HEK-293) cells. Among these, complex **2** exhibited the strongest activity toward HT-29 cells with an IC_{50} of 3.59 ± 0.72 μM. The results confirmed that cell death occurred through mitochondrial dysfunction-mediated apoptosis.[43] The anticancer potential of the synthesized adamantane-based complexes was comparatively evaluated against previously reported results, as shown in Fig. 4.

Long-term proliferative inhibition in A375 melanoma cells by ruthenium complex RuAD1

The colony formation assay enables extended observations under low cell density, primarily providing insights into long-term proliferative potential. A colony formation assay was performed on A375 melanoma cancer cells to assess long-term proliferative capacity under low-density conditions. Cells were seeded at a density of 2×10^3 in a 6-well plate and treated with varying concentrations of the ruthenium complex containing the adamantane-thiourea ligand (**RuAD1**). After a 2-day incubation period, the medium was refreshed every three days until the seventh day. The results consistently demonstrated the substantial cytotoxic effects of **RuAD1** on dose-dependent cancer cells. The dependent experiment for the ruthenium complex **RuAD1** was subsequently conducted using the colony formation assay, with specified concentrations (0, 5, 10, 15 μM). The results revealed a marked inhibitory effect on cell

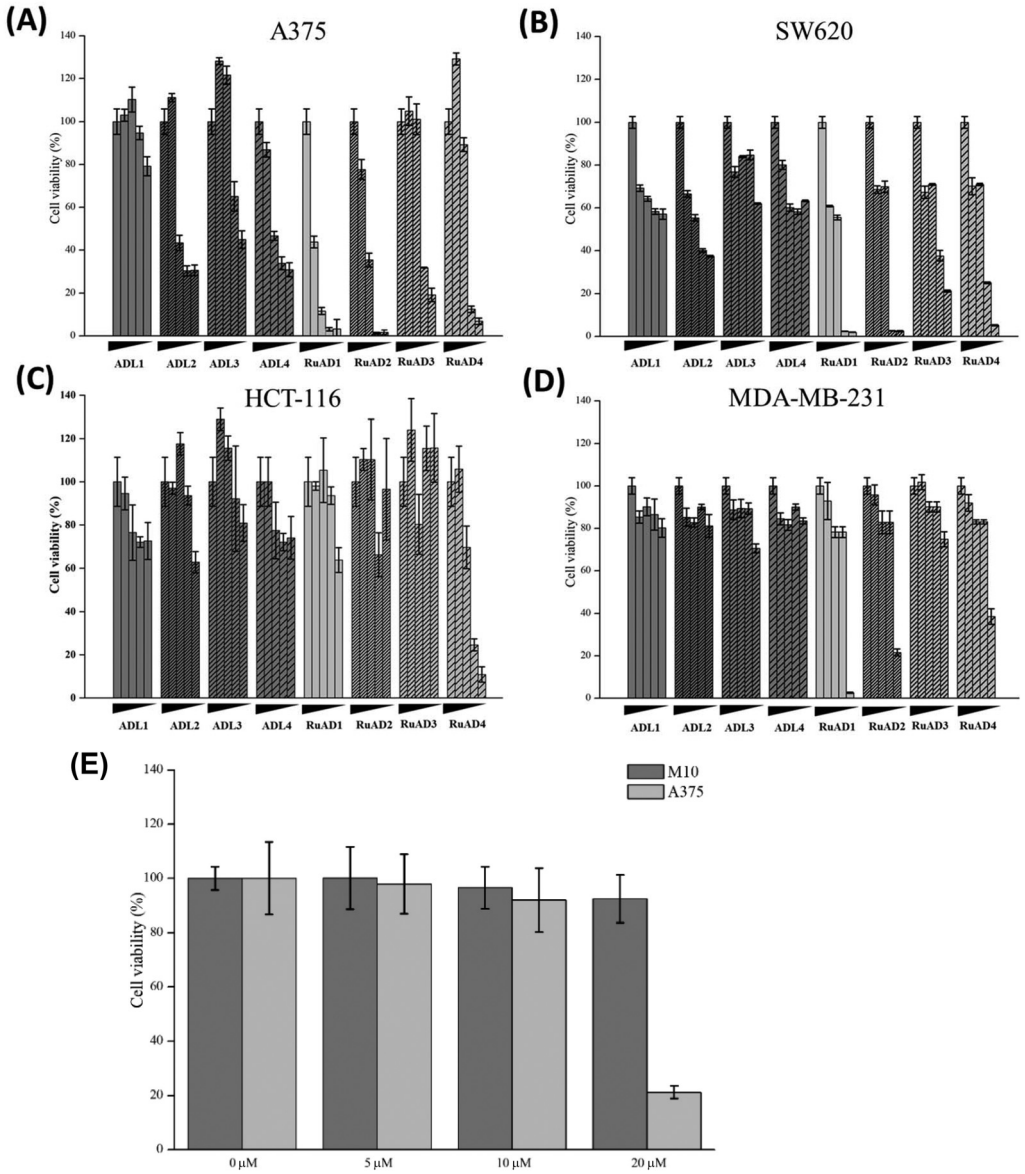

Fig. 3 The cell viability of (A) melanoma A375 cells, (B) colon cancer SW620 cells, (C) colon cancer cells HCT116, and (D) breast cancer MDA-MB-231 treated with complexes (0–100 μM) for 48 h. (E) Cytotoxic effect of **RuAD1** on the cell viability against A375 cancer cells and M10 normal cells.

Table 2 *In vitro* cytotoxicity (IC_{50} values in μM) of AD-thiourea ligands and Ru-AD-thiourea complexes for 48 h[a]

Entry	Compound	A375	SW620	MDA-MB-231	HCT116	M10
1.	**ADL1**	>200	>200	>200	>200	
2.	**ADL2**	19.1	25.2	>200	>200	
3.	**ADL3**	62.2	>200	>200	>200	
4.	**ADL4**	18.5	>200	>200	>200	
5.	**RuAD1**	9.3	17.1	68.2	>200	>100
6.	**RuAD2**	15.9	25.3	76.4	>200	
7.	**RuAD3**	42.1	36.4	>200	>200	
8.	**RuAD4**	22.3	29.1	84.9	27.3	
9.	Cisplatin[b]	57.8	>100	>100	>100	

[a] Non-linear regression analysis of 50% inhibitory concentration determined by taking the mean value of $n = 3$ independent MTS assay experiments; treatment time: 48 h. A375 are human melanoma cancer cells. MDA-MB-231 are human breast cancer cells. HCT-116 and SW620 are human colon cancer cells. H184B5F5/M10 (M10) are normal breast cells. [b] Cisplatin was used as a reference drug.

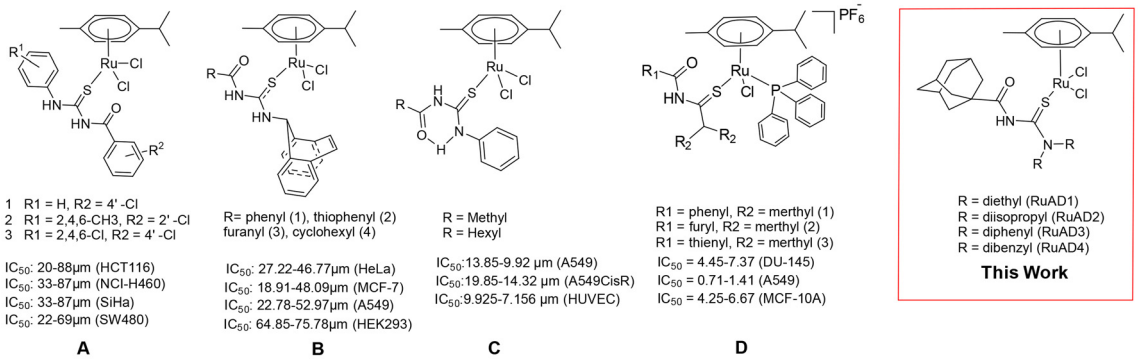

Fig. 4 Representative structures of previously reported acylthiourea-based organoruthenium complexes **A**,[24] **B**,[22] **C** [23] and **D** [9] exhibiting significant anticancer activity across various cancer cell lines.

proliferation beginning at 15 μM (Fig. 5). These results indicated that complex **RuAD1** exhibited notable growth inhibitory effects on human melanoma A375 cells in a dose-dependent manner, whereas cisplatin displayed only weak inhibitory effects.

Inhibitory effects of RuAD1 on migration in A375 melanoma cells

To investigate whether **RuAD1** treatment could influence the migration of A375 melanoma cells, migration assays were performed. Results showed that A375 cells exposed to 10 μM **RuAD1** had significantly reduced cell density after 48 hours compared to the control group. The calculated denuded zone, indicating the migratory ability of A375 cells treated with **RuAD1**, was 90% at 24 h and 63% at 48 h, suggesting that **RuAD1** effectively inhibits migration of the human melanoma cell line in a time-dependent manner (Fig. 6).

Induction of apoptotic morphological changes in A375 cells by RuAD1 treatment

The morphological changes, including number reduction, shrinkage, and rounding of cells, which are hallmarks of apoptosis, were observed in A375 cells following the treat-

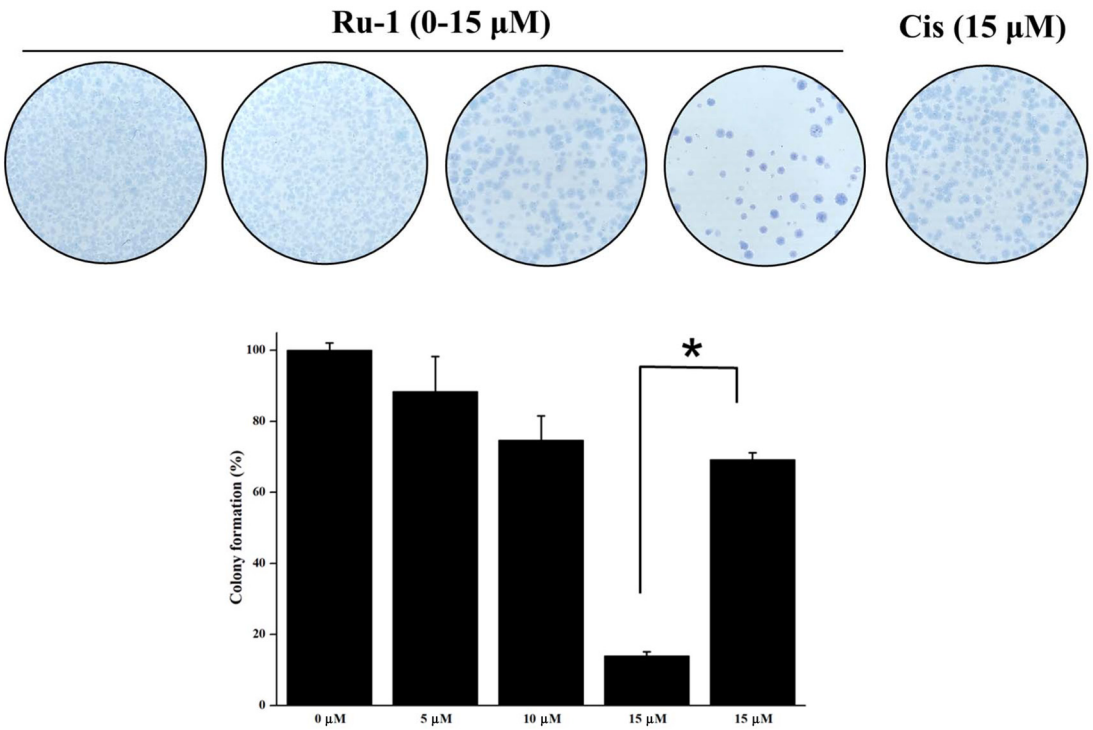

Fig. 5 Colony formation of A375 melanoma skin cancer cells treated with **RuAD1** and cisplatin (**CIS**) for 72 h and refreshed medium for one week.

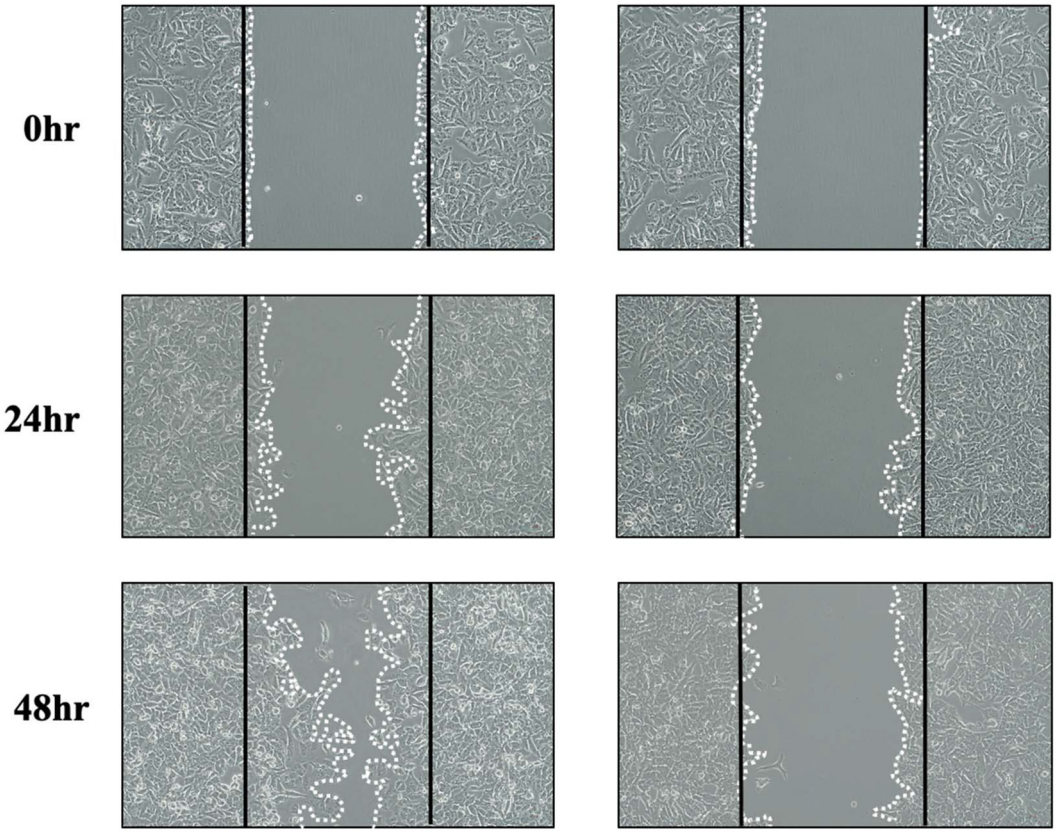

Fig. 6 The cell migration effect on A375 melanoma skin cancer cells treated with **RuAD1** for 0–48 h.

ment with complex **RuAD1** (0, 5, 10, and 20 μM) for 48 h. The cytotoxic **RuAD1** induced a significant change in cellular morphology, which confirmed the high activity of **RuAD1**. The IC_{50} value for complex **RuAD1** against A375 human melanoma cancer cell lines was around 9.3 μM. The cell morphology in the A375 treated with **RuAD1** gradually transitioned to a shrunken state, with debris appearing in the surrounding area. Black arrows indicate granular apoptotic cells, which increased in number with time and higher concentrations of **RuAD1**, suggesting that **RuAD1** may induce apoptosis in cancer cells (Fig. 7).

RuAD1 induced the mitochondrial apoptotic pathway in A375 cells

The proteins of the Bcl-2 family are pivotal regulators of apoptosis. Pro-apoptotic protein Bax facilitates the release of mitochondrial cytochrome c, promoting apoptosis, which culminates in cell death through the activation of caspase proteins.[44] Conversely, anti-apoptotic proteins such as Bcl-2 inhibit apoptosis by interacting with pro-apoptotic counterparts. In this study, western blot analysis was employed to evaluate the expression levels of the Bcl-2 family and caspase proteins in A375 cells treated with **RuAD1** at concentrations of

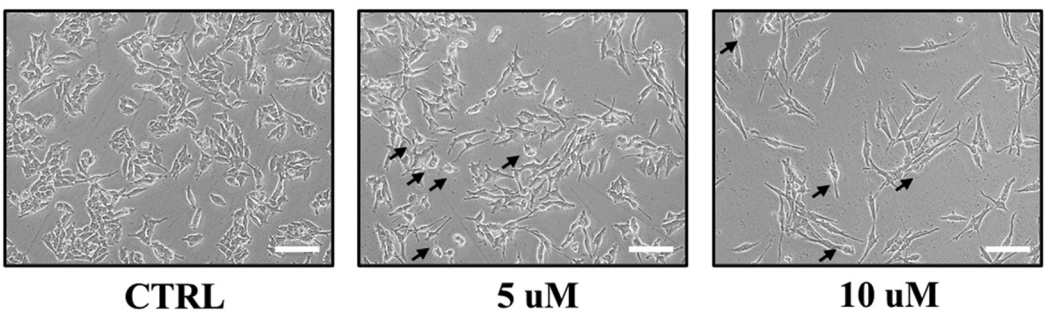

Fig. 7 The cell morphology changes and apoptotic body formation of A375 melanoma skin cancer cells treated with **RuAD1** for 48 h.

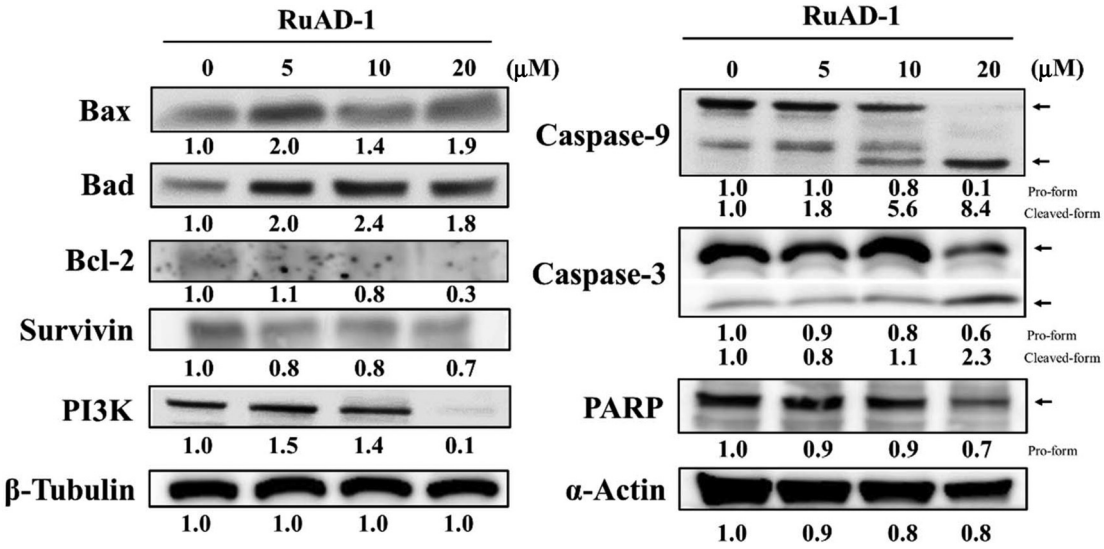

Fig. 8 Western blot analysis showing that **RuAD1** induced the Bax/Bcl-2-mediated apoptotic pathway in A375 melanoma skin cancer cells.

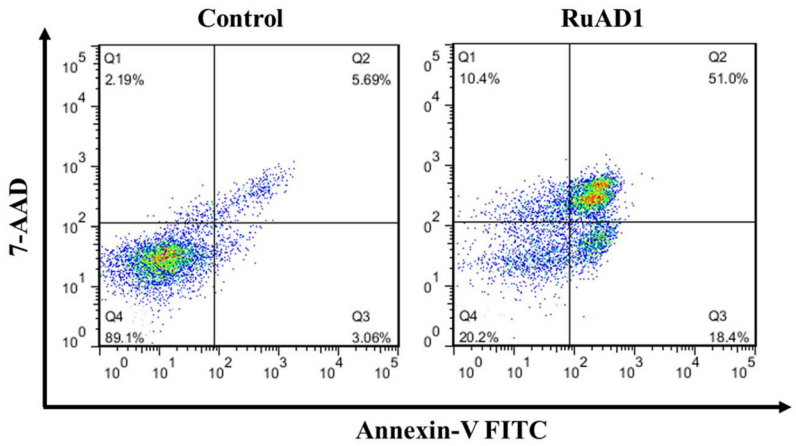

Fig. 9 Quantification of apoptotic cell death induced by complex **RuAD1** using the Annexin V-FITC/7AAD double-staining assay of A375 cells for 48 h.

0, 5, 10, and 20 μM. The assessed proteins included Bcl-2, Bcl-XL, Bax, XIAP, cleaved caspase-9, cleaved caspase-3, and PARP. Following 48 hours of **RuAD1** treatment, a marked decrease in the expression of anti-apoptotic proteins Bcl-2 and XIAP was observed, while an increase in pro-apoptotic Bax and Bad indicated that **RuAD1** mediates apoptosis through the modulation of Bcl-2 family proteins (Fig. 8). Furthermore, analysis of downstream apoptotic markers revealed increased levels of cleaved caspase-9 and cleaved caspase-3, accompanied by a decrease in the pro-form of PARP. These results indicated that **RuAD1**-induced apoptosis in A375 cells is related to the mitochondrial pathway (Fig. 9).

RuAD1-induced apoptotic cell death in A375 melanoma cells

A flow cytometric assay was performed to evaluate apoptosis in A375 cells treated with **RuAD1** using Annexin V-FITC/7-AAD staining. As shown in Fig. 9, the proportion of viable cells (Q4) decreased from 89.1% in the control to 20.3% following **RuAD1** treatment. Notably, **RuAD1** promoted apoptotic cell death, with the early apoptotic population (Q3) increasing from 3.06% to 18.4% and the late apoptotic population (Q2) markedly elevated from 5.69% to 51.7%. These results indicated that **RuAD1** induced A375 melanoma cell death predominantly through the apoptotic pathway.

Conclusion

Ru(η^6-*p*-cymene) complexes (**RuAD1–RuAD4**) containing adamantane-based acylthiourea ligands (**ADL1–ADL4**) were synthesized and characterized. The molecular structure of complexes **RuAD1–RuAD4** was confirmed by a single-crystal XRD study. The biological activities of all compounds were evaluated against human melanoma (A375), triple-negative breast

cancer (MDA-MB-231), and colon cancer (HCT116 and SW620) cell lines. All ruthenium complexes demonstrated greater growth inhibition than their respective ligands, with **RuAD1** showing the strongest cytotoxicity against A375 cells (IC_{50} = 9.3 ± 1.2 μM) while maintaining lower toxicity toward normal M10 cells. Migration assays revealed that **RuAD1** treatment (10 μM) significantly inhibited A375 migration in a time-dependent manner, with a 90% denuded zone at 24 hours and 63% at 48 hours compared to the control. Treatment of A375 cells with **RuAD1** (0, 5, 10, and 20 μM) for 48 h induced morphological changes characteristic of apoptosis. Furthermore, western blot analysis showed that **RuAD1** treatment reduced anti-apoptotic proteins (Bcl-2 and XIAP) and increased pro-apoptotic proteins (Bax and Bad) in A375 cells, along with activation of caspase-9, caspase-3, and PARP cleavage, indicating that **RuAD1** induces apoptosis *via* the mitochondrial pathway (Fig. 10). According to *in silico* ADMET analysis, **RuAD1** showed the best predicted pharmacokinetic properties, including good absorption, strong protein binding, no major metabolism issues, and suitability for oral use. Adamantane organometallic ruthenium complexes with thiourea groups represent a promising area of research in anticancer drug development. Their unique structural features and potential for selective toxicity warrant further investigation to understand their full therapeutic potential and mechanisms of action. As research progresses, these complexes may pave the way for new treatments in oncology.

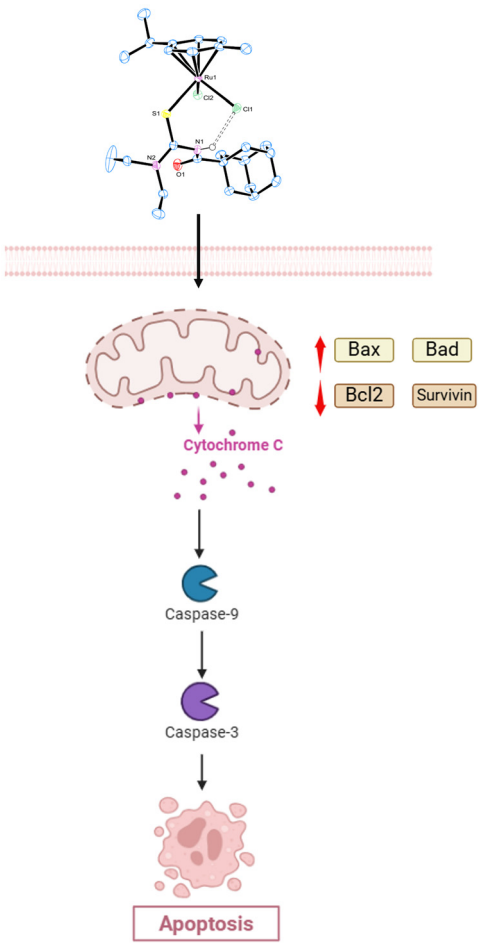

Fig. 10 The proposed anticancer mechanisms of **RuAD1** *via* the mitochondrial apoptotic pathway in A375 cells.

Experimental section

Materials and structural characterization

FT-IR spectra of each compound were recorded by first dissolving the samples in CH_2Cl_2, depositing the solution onto a NaCl plate, and allowing the solvent to evaporate to form a thin film. The film was then covered with another NaCl plate prior to measurement in the 4000–400 cm^{-1} range. Spectra were collected on a Bruker Optics FT-IR Alpha OPUS spectrometer. NMR spectra were recorded on a Jeol 400 MHz spectrometer using tetramethylsilane (TMS) as an internal standard for ^1H and ^{13}C NMR. Chemical shifts (δ) were reported in ppm relative to the residual solvent signal ($CDCl_3$: δ = 7.26 in ^1H NMR; δ = 77.0 in ^{13}C NMR; DMSO-d^6: δ = 2.50 in ^1H NMR; δ = 39.5 in ^{13}C NMR). Ultraviolet–visible (UV–vis) spectra were obtained using an Agilent 8453 spectrophotometer. Elemental analyses were performed on a Unicube elemental analyzer. HR-MS was performed on an Orbitrap mass spectrometer with a resolving power of 120 000 (FWHM).

Synthesis and characterization of the ligands (ADL1–ADL4) and their complexes RuAD1–RuAD4

2.00 mmol (0.397 g) of 1-adamantanecarbonyl chloride was dissolved in 50 mL of anhydrous acetone. Subsequently, 2.05 mmol (0.200 g) of potassium thiocyanate solution was added to the above solution and refluxed for 1 hour. After cooling, 2.05 mmol of corresponding amines **L1–L4** (**L1**: 0.092, **L2**: 0.105, **L3**: 0.127, and **L4**: 0.136 g) was added, and the mixture was stirred for 4 hours. The progress of the reaction was monitored by thin-layer chromatography (TLC). Upon completion, HCl (1.0 N, 3.0 mL) and distilled water (100 mL) were added to the mixture, resulting in the formation of a white precipitate for all compounds except **L3**, which formed a yellow precipitate. The products were washed thoroughly with water and dried under vacuum, as illustrated in Scheme 2A.

ADL1. *N*-(Diethylcarbamothioyl)adamantane-1-carboxamide, white solid. Yield: 97.6%. Mp: 168.0 °C. UV–vis (MeOH): λ_{max}, nm (ε, dm^3 mol^{-1} cm^{-1}) 203 (22 988), 224 (5340), 280 (11 303). FT-IR (thin film, cm^{-1}): 3280 (m; ν(amide N–H)), 2892, 2849 (s; ν(AD, C–H)), 1642 (s; ν(C═O)), 1235 (m; ν(C═S)). ^1H NMR (400 MHz, $CDCl_3$): δ, ppm, 7.65 (s, 1H, thiocarbonyl, N–***H***), 3.95 (b s, 2H, N–C$\boldsymbol{H}_2$), 3.45 (b s, 2H, N–C$\boldsymbol{H}_{2b}$), 2.06 (s, 3H, adamantane protons), 1.89–1.88 (d, 6H, J = 2.5 Hz, adamantane protons), 1.77–1.67 (m, 6H, adamantane protons), 1.29–1.23 (b, 6H, amine, C$\boldsymbol{H}_{3c}$). ^{13}C NMR (100 MHz, $CDCl_3$): δ, ppm, 179.88 (***C***═S), 174.32 (***C***═O), 48.11, 47.64 (N***C***$_c$H$_2$ (CH_3)), 41.71, 38.88, 36.35, 28.03 (***C***$_{i\text{-}AD}$), 13.30, 11.62 (NCH_2 (***C***$_d$H$_3$)). HR-MS (m/z) [found (calcd)]: 295.18378 (295.1844) [L + H^+]$^+$,

317.16574 (317.1664) $[L + Na]^+$ and 611.34198 (611.3430) $[2L + Na]^+$.

ADL2. *N*-(Diisopropylcarbamothioyl)adamantane-1-carboxamide, white solid. Yield: 83.5%. Mp: 139.8 °C. UV–vis (MeOH): λ_{max}, nm (ε, $dm^3\ mol^{-1}\ cm^{-1}$) 206 (4886), 227 (3274), 282 (10 970). FT-IR (thin film, cm^{-1}): 3290 (m; ν(amide N–H)), 2902, 2847 (s; ν(AD, C–H)), 1656 (s; ν(C═O)), 1219 (m; ν(C═S)). ^{1}H NMR (400 MHz, $CDCl_3$): δ, ppm, 7.38 (s, 1H, thiocarbonyl, N–***H***), 4.18 (*b s*, 2H, N–C***H***$_b$), 2.06 (s, 3H, adamantane protons), 1.89 (d, 6H, adamantane protons), 1.76–1.68 (m, 6H, adamantane protons), 1.64–1.11 (b, 12H, amine, (C***H***$_{3c}$)$_4$). ^{13}C NMR (100 MHz, $CDCl_3$): δ, ppm, 178.97 (***C***═S), 174.86 (***C***═O), 55.32, 51.00 (N–***C***H), 41.59, 38.93, 36.39, 28.07 (C-AD), 19.93 (N–CH–(CH$_3$)$_2$). HR-MS (*m*/*z*) [found (calcd)]: 323.21512 (323.2157) $[L + H^+]^+$, 345.19693 (345.1977) $[L + Na]^+$ and 667.40784 (667.4055) $[2L + Na]^+$.

ADL3. *N*-(Diphenylcarbamothioyl)adamantane-1-carboxamide, yellow solid. Yield: 50.7%. Mp: 137.3 °C. UV–vis (MeOH): λ_{max}, nm (ε, $dm^3\ mol^{-1}\ cm^{-1}$) 211 (34 541), 254 (9258), 309 (7646). FT-IR (thin film, cm^{-1}): 3341 (m; ν(amide N–H)), 2906, 2849 (s; ν(AD, C–H)), 1709 (s; ν(C═O)), 1213 (m; ν(C═S)). ^{1}H NMR (400 MHz, $CDCl_3$): δ, ppm, 8.11 (s, 1H, thiocarbonyl, N–***H***), 7.37–7.25 (m, 10H, N–(C$_6$***H***$_{5b}$)$_2$), 1.96 (s, 3H, adamantane protons), 1.68–1.56 (m, 12H, adamantane protons). ^{13}C NMR (100 MHz, $CDCl_3$): δ, ppm, 183.21 (***C***═S), 172.36 (***C***═O), 145.82, 129.20, 127.40, 127.09 (amine, phenyl), 41.64, 38.52, 36.23, 27.87 (***C***-AD). HR-MS (*m*/*z*) [found (calcd)]: 391.18372 (391.1844) $[L + H^+]^+$, 413.16553 (413.1664) $[L + Na]^+$ and 803.34186 (803.3430) $[2L + Na]^+$.

ADL4. *N*-(Dibenzylcarbamothioyl)adamantane-1-carboxamide, white solid. Yield: 93.8%. Mp: 158.8 °C. UV–vis (MeOH): λ_{max}, nm (ε, $dm^3\ mol^{-1}\ cm^{-1}$) 213 (31 183), 223 (11 386), 284 (12 466). FT-IR (thin film, cm^{-1}): 3276 (m; ν(amide N–H)), 2900, 2847 (s; ν(AD, C–H)), 1689 (s; ν(C═O)), 1195 (m; ν(C═S)). ^{1}H NMR (400 MHz, $CDCl_3$): δ, ppm, 7.96 (s, 1H, thiocarbonyl, N–***H***), 7.37–7.08 (m, 10H, N–CH$_2$–(C$_6$***H***$_{5c}$)$_2$), 5.15 (b s, 2H, N–C***H***$_{2b}$(C$_6$H$_5$)), 4.57 (b s, 2H, N–C***H***$_{2b}$(C$_6$H$_5$)), 2.08 (s, 3H, adamantane protons), 1.91–1.90 (d, 6H, adamantane protons), 1.78–1.68 (m, 6H, adamantane protons). ^{13}C NMR (100 MHz, $CDCl_3$): δ, ppm, 182.54 (***C***═S), 174.58 (***C***═O), 135.53, 134.76, 128.95, 128.20, 127.87 (amine, aromatic rings), 56.55, 55.88 (N–***C***H), 41.93, 38.94, 36.35, 28.05 (***C***-AD). HR-MS (*m*/*z*) [found (calcd)]: 419.21487 (419.2157) $[L + H^+]^+$, 441.1977 (441.19681) $[L + Na]^+$, and 859.40454 (859.4055) $[2L + Na]^+$.

The **RuAD1–RuAD4** complexes were prepared by reacting 0.327 mmol of **ADL1–ADL4** (**ADL1**: 0.092, **ADL2**: 0.105, **ADL3**: 0.127, and **ADL4**: 0.136 mg) with $[RuCl_2(\eta^6\text{-}p\text{-cymene})]_2$ (0.100 g, 0.163 mmol) in 10 mL of toluene solution along with a few drops of MeOH, while stirring for 4 hours. After forming an orange solution, 90 mL of hexane was added to the solution, and the mixture was stored in a refrigerator overnight. This led to the formation of an orange solid, which was then subjected to filtration, washed with hexane, and dried *in vacuo*, as illustrated in Scheme 2B.

RuAD1. [Dichloro(*p*-cymene)(*N*-(diethylcarbamothioyl)adamantane-1-carboxamide)ruthenium(II)], orange solid. Yield: 87.8%. Mp: 135.7 °C. Molecular formula: $C_{26}H_{40}Cl_2N_2ORuS$. UV–vis (MeOH): λ_{max}, nm (ε, $dm^3\ mol^{-1}\ cm^{-1}$) 257 (17 606), 427 (658). FT-IR (thin film, cm^{-1}): 3139 (m; ν(amide N–H)), 2904, 2847 (s; ν(AD, C–H)), 1699 (s; ν(C═O)), 1209 (m; ν(C═S)). ^{1}H NMR (400 MHz, $CDCl_3$): δ, ppm, 10.01 (s, 1H, thiocarbonyl, N–***H***), 5.44–5.42 (d, J = 5.9 Hz, 2H, *p*-cymene aromatic-***H***$_e$), 5.20–5.19 (d, J = 5.9 Hz, 2H, *p*-cymene aromatic-***H***$_e$), 4.05–4.02 (*q*, J = 6.9 Hz, 2H, N–C***H***$_2$), 3.34–3.29 (*q*, J = 6.9 Hz, 2H, N–C***H***$_2$), 3.01–2.95 (hept, J = 6.9 Hz, 1H, –C***H***$_f$(CH$_3$)$_2$), 2.23 (s, 3H, C***H***$_{3d}$), 2.06 (s, 3H, adamantane protons), 1.98 (d, J = 2.7 Hz, 6H, adamantane protons), 1.72–1.71 (m, 6H, J = 2.7 Hz, adamantane protons), 1.41–1.38 (t, J = 6.9 Hz, 3H, N–CH$_2$–C***H***$_3$), 1.33–1.32 (d, J = 6.9 Hz, 6H, *p*-cymene, CH(C***H***$_{3f}$)$_2$), 1.22–1.19 (t, J = 6.9 Hz, 3H, N–CH$_2$–C***H***$_3$). ^{13}C NMR (100 MHz, $CDCl_3$): δ, ppm, 182.04 (***C***$_b$═S), 177.61 (***C***$_a$═O), 103.53, 100.25, 84.52, 82.00, 30.75, 22.45, 18.71 (*p*-cymene), 48.18, 47.72 (N***C***H$_2$ (CH$_3$)), 42.88, 39.14, 36.45, 28.11 (***C***$_i$-AD), 30.76 (N–***C***H–(CH$_3$)$_2$), 22.45 (cymene-***C***H$_3$), 18.71 (–CH–(***C***H$_3$)$_2$), 12.57, 12.06 (NCH$_2$(***C***H$_3$)). HR-MS (*m*/*z*) [found (calcd)]: 529.1819 (529.1859) [M-HCl-Cl$^-$]$^+$.

RuAD2. [Dichloro(*p*-cymene)(*N*-(diisopropylcarbamothioyl) adamantane-1-carboxamide)ruthenium(II)], orange solid. Yield: 71%. Mp: 131.5 °C. Molecular formula: $C_{28}H_{44}Cl_2N_2ORuS$. UV–vis (MeOH): λ_{max}, nm (ε, $dm^3\ mol^{-1}\ cm^{-1}$) 230 (17 134), 257 (15 046), 327 (4180), 432 (1036). FT-IR (thin film, cm^{-1}): 3129 (m; ν(amide N–H)), 2910, 2847 (s; ν(AD, C–H)), 1697 (s; ν(C═O)), 1207 (m; ν(C═S)). ^{1}H NMR (400 MHz, $CDCl_3$): δ, ppm, 9.84 (s, 1H, thiocarbonyl, N–***H***), 5.45–5.43 (d, J = 6.1 Hz, 2H, *p*-cymene aromatic-***H***$_e$), 5.20–5.19 (b, 2H, *p*-cymene aromatic-***H***$_e$), 4.16–4.09 (hept, J = 6.6 Hz, 2H, N–C–***H***$_b$), 3.02–2.92 (hept, J = 6.9 Hz, 1H, *p*-cymene, C***H***$_f$(CH$_3$)$_2$), 2.24 (s, 3H, *p*-cymene, C***H***$_{3d}$), 2.08 (s, 3H, adamantane protons), 1.99 (d, J = 2.7 Hz, 6H, adamantane protons), 1.73 (m, 6H, J = 2.7 Hz, adamantane protons), 1.47 (m, 12H, N–CH$_b$(C***H***$_{3c}$)$_4$), 1.34–1.32 (d, J = 6.9 Hz, 6H, *p*-cymene, CH (C***H***$_{3g}$)$_2$). ^{1}H NMR (400 MHz, DMSO-d$_6$): δ, ppm, 9.17 (s, 1H, thiocarbonyl, N–***H***), 5.82–5.80 (d, J = 6.4 Hz, 2H, *p*-cymene aromatic-***H***$_e$), 5.78–5.76 (d, J = 6.4 Hz, 2H, *p*-cymene aromatic-***H***$_e$), 4.15 (m, 2H, N–C–***H***$_b$), 2.88–2.77 (hept, J = 6.9 Hz, 1H, *p*-cymene, C***H***$_f$(CH$_3$)$_2$), 2.08 (s, 3H, *p*-cymene, C***H***$_{3d}$), 1.97 (s, 3H, adamantane protons), 1.81–1.80 (d, J = 2.9 Hz, 6H, adamantane protons), 1.66 (m, 6H, adamantane protons), 1.42 (m, 12H, N–CH$_b$(C***H***$_{3c}$)), 1.20–1.18 (d, J = 6.9 Hz, 6H, *p*-cymene, CH (C***H***$_{3g}$)$_2$). ^{13}C NMR (100 MHz, $CDCl_3$): δ, ppm, 181.95 (***C***═S), 178.41 (***C***═O), 103.67, 100.66, 84.25, 81.74, 22.47, 18.92 (*p*-cymene), 42.84, 39.25, 36.45, 28.12 (***C***$_{I\text{-}AD}$), 30.96 (N–***C***H–(CH$_3$)$_2$), 22.47 (N***C***$_c$H(CH$_3$)$_2$), 20.51, 19.51(N***C***$_c$H(CH$_3$)$_2$), 18.92 (*C*H(***C***$_d$H$_3$)$_2$). HR-MS (*m*/*z*) [found (calcd)]: 557.2132 (557.2172) [M-HCl-Cl$^-$]$^+$.

RuAD3. [Dichloro(*p*-cymene)(*N*-(diphenylcarbamothioyl)adamantane-1-carboxamide) ruthenium(II)], orange solid. Yield: 75%. Mp: 159.8 °C. Molecular formula: $C_{34}H_{40}Cl_2N_2ORuS$. UV–vis (MeOH): λ_{max}, nm (ε, $dm^3\ mol^{-1}\ cm^{-1}$) 257 (19 100), 299 (13 275), 434 (1150). FT-IR (thin film, cm^{-1}): 3110 (m; ν(amide N–H)), 2908, 2851 (s; ν(AD, C–H)), 1715 (s; ν(C═O)), 1207 (m; ν(C═S)). ^{1}H NMR (400 MHz, $CDCl_3$): δ, ppm, 10.73

(s, 1H, thiocarbonyl, N–***H***), 7.34–7.15 (m, 10H, N–(C_6***H***$_{5b}$)$_2$), 5.37–5.36 (d, J = 6.4 Hz, 2H, *p*-cymene aromatic-***H***$_d$), 5.19–5.18 (d, J = 6.4 Hz, 2H, *p*-cymene aromatic-***H***$_d$), 2.91–2.80 (hept, J = 7.0 Hz, 1H, *p*-cymene, C***H***$_e$(CH_3)$_2$), 2.20 (s, 3H, *p*-cymene, C***H***$_{3c}$), 1.90 (s, 3H, adamantane protons), 1.58 (d, J = 2.7 Hz, 6H, adamantane protons), 1.25 (m, 6H, J = 2.7 Hz, adamantane protons), 1.25–1.24 (d, J = 7.0 Hz, 6H, *p*-cymene, CH(C***H***$_{3f}$)$_2$). ^{1}H NMR (400 MHz, DMSO-d_6): δ, ppm, 10.07 (s, 1H, thiocarbonyl, N–***H***), 7.39–7.16 (m, 10H, N–(C_6***H***$_{5b}$)$_2$), 5.82–5.81 (d, J = 6.4 Hz, 2H, *p*-cymene aromatic-***H***$_d$), 5.78–5.76 (d, J = 6.4 Hz, 2H, *p*-cymene aromatic-***H***$_d$), 2.88–2.78 (hept, J = 7.0 Hz, 1H, *p*-cymene, C***H***e(CH_3)$_2$), 2.09 (s, 3H, *p*-cymene, C***H***$_{3c}$), 1.87–1.45 (m, 15H, adamantane protons), 1.20–1.18 (d, J = 7.0 Hz, 6H, *p*-cymene, CH(C***H***$_{3f}$)$_2$). ^{13}C NMR (100 MHz, $CDCl_3$): δ, ppm, 187.09 (***C***=S), 175.19 (***C***=O), 145.52, 129.37, 127.74, 127.03 (amine, phenyl), 103.53, 100.67, 84.71, 82.63, 22.41, 18.69 (*p*-cymene), 42.49, 38.30, 36.33, 27.93 (***C***$_{k\text{-}AD}$), 30.67 (N–***C***H–(CH_3)$_2$). HR-MS (*m*/*z*) [found (calcd)]: 625.1818 (625.1859) [M-HCl-Cl$^-$]$^+$.

RuAD4. [Dichloro(*p*-cymene)(*N*-(dibenzylcarbamothioyl)adamantane-1-carboxamide)ruthenium(II)], orange solid. Yield: 78.8%. Mp: 176.0 °C. Molecular formula: $C_{36}H_{44}Cl_2N_2ORuS$. UV–vis (MeOH): λ_{max}, nm (ε, dm^3 mol^{-1} cm^{-1}) 260 (20 752), 427 (666). FT-IR (thin film, cm^{-1}): 3119 (m; ν(amide N–H)), 2906, 2849 (s; ν(AD, C–H)), 1703 (s; ν(C=O)), 1191 (m; ν(C=S)). ^{1}H NMR (400 MHz, $CDCl_3$): δ, ppm, 10.57 (s, 1H, thiocarbonyl, N–***H***), 7.35–7.05 (m, 10H, N–(C_6***H***$_{5b}$)$_2$), 5.38–5.36 (d, J = 5.8 Hz, 2H, *p*-cymene aromatic-***H***$_d$), 5.19–5.18 (d, J = 5.8 Hz, 2H, *p*-cymene aromatic-***H***$_d$), 5.03 (b, 2H, amine, N–C**H**$_2$), 4.40 (b, 2H, N–C**H**$_2$), 2.73–2.63 (hept, J = 6.9 Hz, 1H, *p*-cymene, C***H***$_e$(CH_3)$_2$), 2.13 (s, 3H, *p*-cymene, C***H***$_{3c}$), 2.06 (s, 3H, adamantane protons), 2.04 (d, J = 2.7 Hz, 6H, adamantane protons), 1.72 (m, 6H, J = 2.7 Hz, adamantane protons), 1.22–1.20 (d, J = 6.9 Hz, 6H, *p*-cymene, CH(C***H***$_{3f}$)$_2$). ^{1}H NMR (400 MHz, DMSO-d_6): δ, ppm, 9.91 (s, 1H, thiocarbonyl, N–***H***), 7.42–7.19 (m, 10H, N–(CH_2(C_6***H***$_5$))$_2$), 5.82–5.81 (d, J = 4.00 Hz, 2H, *p*-cymene aromatic-***H***$_e$), 5.78–5.76 (d, J = 8.00 Hz, 2H, *p*-cymene aromatic-***H***$_e$), 5.12, 4.52 (s, 4H, N–C***H***$_{2b}$(C_6H_5)), 2.88–2.77 (*q*, J = 7.0 Hz, 1H, *p*-cymene, C***H***$_f$(CH_3)$_2$), 2.08 (s, 3H, *p*-cymene, C***H***$_{3d}$), 1.97 (s, 3H, J = 2.5 Hz, adamantane protons), 1.85–1.84 (m, J = 2.5 Hz, 6H, adamantane protons), 1.65 (m, 6H, adamantane protons), 1.20–1.18 (d, J = 7.0 Hz, 6H, *p*-cymene, CH(C***H***$_{3g}$)$_2$). ^{13}C NMR (100 MHz, $CDCl_3$): δ, ppm, 184.21 (***C***=S), 177.92 (***C***=O), 134.5, 134.21, 129.22, 128.96, 128.76, 128.67, 127.91 (amine, aromatic rings), 103.40, 100.79, 84.57, 82.11, 30.65, 22.40, 18.62 (*p*-cymene), 43.17, 39.12, 36.40, 28.14 (***C***$_{h\text{-}AD}$), 30.65 (N–***C***H–(CH_3)$_2$). HR-MS (*m*/*z*) [found (calcd)]: 653.2132 (653.2172) [M-HCl-Cl$^-$]$^+$.

Single-crystal X-ray diffraction study

Single crystals of the complexes (**RuAD1–RuAD4**) were grown by slow evaporation of their $CDCl_3$ solutions. Olex2 was employed for the final data presentation and structure plots. All X-ray diffraction data were accumulated using Rigaku Oxford Diffraction single-crystal X-ray diffractometers with Mo Kα radiation (λ = 0.71073 Å). Data collection was executed using the CrysAlisPro 1.171.41.56a program. Cell refinement and data reduction were achieved using the CrysAlisPro 1.171.41.56a program. The structure was determined using the Olex2/ShelXL program and refined using full-matrix least squares. All non-hydrogen atoms were refined anisotropically, whereas hydrogen atoms were placed at calculated positions and included in the final refinement stage with fixed parameters.

ADMET studies

Ligands and complexes were evaluated for *in silico* ADMET prediction, including aqueous solubility, blood–brain barrier penetration, human intestinal absorption, plasma protein binding, cytochrome P450 interactions, and potential toxicity, using the ADMET descriptors module in Discovery Studio 2022 (BIOVIA, Dassault Systèmes, San Diego, USA).[45]

Cytotoxicity experiments

Cell culture. Human melanoma A375 cells, triple-negative breast cancer MDA-MB-231 cells, and colon cancer HCT116 and SW620 cells were obtained from the American Type Culture Collection (ATCC; Manassas, VA, USA). The human normal mammary epithelial H184B5F5/M10 (M10) cells were kindly provided by Dr Chien-Chih Chiu from the Department of Biotechnology, Kaohsiung Medical University (Kaohsiung, Taiwan). The A375 and MDA-MB-231 cells were maintained in DMEM (Dulbecco's modified Eagle's medium) supplemented with 10% FBS (fetal bovine serum), and antibiotics (100 units per mL penicillin and 100 μg mL^{-1} streptomycin) at 37 °C under a humidified atmosphere of 5% CO_2. In addition, the completed cultured medium for HCT116, SW620 and M10 cells was DMEM/F12/FBS (10%)/antibiotics (1%), and DMEM/FBS (10%)/antibiotics (1%), respectively.

Cytotoxicity assay. The cytotoxicity of **ADL1–ADL4** and **RuAD1–RuAD4** was studied by using the MTS [3-(4,5-dimethylthiazol-2-yl)-5-(3-carboxymethoxyphenyl)-2-(4-sulfophenyl)-2*H*-tetrazolium] assay. All the cell lines were cultured and maintained in the complete culture medium with 5 × 10^3 cells per well being seeded in a 96-well plate and incubated overnight under humidified conditions at 37 °C with 5% CO_2. The cells were treated with adjusted concentrations (0–100 μM) for 48 h. After treatment with compounds, the cells were washed twice with PBS and incubated with diluted fresh MTS media for 4 h. The data were recorded at 490 nm. By using the formula, $A - B/A \times 100$ (A = control group and B = treated group), the cell viability (%) was calculated. Each experimental point represents the mean ± SD of three replicates.

Colon formation assay. Cells were seeded and grown to around 80% confluency and treated with a specific concentration of vehicle, **RuAD1**, or cisplatin (CIS) for 72 h. After 24 h, cells were trypsinized and seeded at about 10 × 10^3 cells in each well of a 6-well plate and allowed to grow for 14 days. Next, the cells were washed with PBS and incubated with 0.5% crystal violet solution (containing 3.7% formaldehyde) for

30 min. Then the crystal violet was washed off with running tap water, and the plates were allowed to dry at room temperature. The image was captured, and the density was measured using ImageJ.

Migration assay. Cells were seeded in 6-well plates and allowed to grow up to 80–90% confluency when a uniform scratch in each well was made with a 10 μL pipette tip. The cells were washed with sterile PBS to remove the debris, and then treated with different concentrations of extract or vehicle for 24 h or 48 h, following which images of the cells were obtained using an inverted microscope. All experiments were repeated three times to record the data.

Western blotting

In brief, 1×10^6 cells were harvested and lysed with lysis buffer (50 mM Tris–HCl, pH 7.5, 137 mM sodium chloride, 1 mM EDTA, 1% Nonidet P-40, 10% glycerol, 0.1 mM sodium orthovanadate, 10 mM sodium pyrophosphate, 20 mM β-glycerophosphate, 50 mM sodium fluoride, 1 mM phenylmethylsulfonyl fluoride, 2 μM leupeptin, and 2 μg mL^{-1} aprotinin) for l h on ice. Lysates were centrifuged at 13 000 rpm for 30 min, and the protein concentration in the supernatant was determined with the bicinchoninic acid (BCA) protein assay kit (Pierce, Rockford, IL, USA). Equal amounts of protein were loaded and separated by SDS-polyacrylamide gel electrophoresis (SDS-PAGE). After electrophoresis, the proteins were electrotransferred to a nitrocellulose membrane (PALL, Ann Arbor, USA), blocked with 5% non-fat milk in TBS-T buffer (TBS containing 0.1% Tween 20) for 1 h and then incubated with corresponding primary antibodies against specific proteins overnight at 4 °C. The blot was washed and incubated with HRP-conjugated secondary antibodies for 1.5 h. The signals were visualized by using an enhanced chemiluminescence (ECL) detection kit (Amersham Piscataway, New Jersey, USA).

Quantification of apoptosis

Annexin V/7-AAD double staining was performed to evaluate phosphatidylserine (PS) externalization, a hallmark of apoptosis. The annexin V/7-AAD kit (Strong Biotech) was used to stain **RuAD1**-treated cells. The cells were detected by flow cytometry (FACSCalibur, BD Biosciences, San Jose, CA) and analyzed by FlowJo v7.5.5 software (Tree Star, Inc., USA).

Statistical analysis

Statistical analysis was performed by using Student's *t*-test for cell assays. The * symbol represents $p < 0.05$ while ** represents $p < 0.01$, where both are considered significant.

Conflicts of interest

There are no conflicts to declare.

Data availability

All supporting data can be obtained from the corresponding author upon request.

Supplementary information (SI): additional crystallographic data, UV–vis, FT-IR, ESI-MS, HR-MS and $^{13}C\{^1H\}$ NMR spectra for all new compounds (**ADL1–ADL4**) and their corresponding Ru(η^6-*p*-cymene) complexes (**RuAD1–RuAD4**). See DOI: https://doi.org/10.1039/d5dt01959a.

CCDC 2447963 (**RuAD1**), 2447682 (**RuAD2**), 2447952 (**RuAD3**) and 2447951 (**RuAD4**) contain the supplementary crystallographic data for this paper.[46a–d]

Acknowledgements

The authors gratefully acknowledge the financial support from the National Science and Technology Council (NSTC), Taiwan (NSTC 114-2113-M-037-006, NSTC 114-2113-M-415-002-MY2 and NSTC 111-2311-B-309-001-MY3), Kaohsiung Medical University (KMU-TB114009), and the NSYSU-KMU Joint Research Project (NSYSUKMU 108-I002). Special thanks are extended to all research group members for their valuable contributions and insightful discussions throughout this study.

References

1 G. H. Ribeiro, A. R. Costa, A. R. de Souza, F. V. da Silva, F. T. Martins, A. M. Plutin and A. A. Batista, An overview on the anticancer activity of Ru(II)/acylthiourea complexes, *Coord. Chem. Rev.*, 2023, **488**, 215161, DOI: 10.1016/j.ccr.2023.215161.

2 T. R. Steel, F. Walsh, A. Wieczorek-Błauż, M. Hanif and C. G. Hartinger, Monodentately-coordinated bioactive moieties in multimodal half-sandwich organoruthenium anticancer agents, *Coord. Chem. Rev.*, 2021, **439**, 213890, DOI: 10.1016/j.ccr.2021.213890.

3 W. D. Tremlett, D. M. Goodman, T. R. Steel, S. Kumar, A. Wieczorek-Błauż, F. P. Walsh, M. P. Sullivan, M. Hanif and C. G. Hartinger, Design concepts of half-sandwich organoruthenium anticancer agents based on bidentate bioactive ligands, *Coord. Chem. Rev.*, 2021, **445**, 213950, DOI: 10.1016/j.ccr.2021.213950.

4 Y. K. Yan, M. Melchart, A. Habtemariam and P. J. Sadler, Organometallic chemistry, biology and medicine: ruthenium arene anticancer complexes, *Chem. Commun.*, 2005, (38), 4764–4776, DOI: 10.1039/B508531B.

5 B. S. Murray, M. V. Babak, C. G. Hartinger and P. J. Dyson, The development of RAPTA compounds for the treatment of tumors, *Coord. Chem. Rev.*, 2016, **306**, 86–114, DOI: 10.1016/j.ccr.2015.06.014.

6 P. V. Sashankh, D. P. Dorairaj, J.-Y. Chen, Y.-L. Chang, K. Chand, R. Karvembu, C.-M. Chien and S. C. Hsu, Synthesis, in silico and in vitro studies of piperazinyl thiourea derivatives as apoptosis inducer for the treatment

of colorectal carcinoma, *J. Mol. Struct.*, 2022, **1262**, 133086, DOI: 10.1016/j.molstruc.2022.133086.

7 A. Saeed, R. Qamar, T. A. Fattah, U. Flörke and M. F. Erben, Recent developments in chemistry, coordination, structure and biological aspects of 1-(acyl/aroyl)-3-(substituted) thioureas, *Res. Chem. Intermed.*, 2017, **43**, 3053–3093, DOI: 10.1007/s11164-016-2811-5.

8 D. P. Dorairaj, J. Haribabu, M. Dharmasivam, R. E. Malekshah, M. K. M. Subarkhan, C. Echeverria and R. Karvembu, Ru(II)-p-Cymene complexes of furoylthiourea ligands for anticancer applications against breast cancer cells, *Inorg. Chem.*, 2023, **62**(30), 11761–11774, DOI: 10.1021/acs.inorgchem.3c00757.

9 B. N. Cunha, L. Luna-Dulcey, A. M. Plutin, R. G. Silveira, J. Honorato, R. R. Cairo, T. D. de Oliveira, M. R. Cominetti, E. E. Castellano and A. A. Batista, Selective coordination mode of acylthiourea ligands in half-sandwich Ru(II) complexes and their cytotoxic evaluation, *Inorg. Chem.*, 2020, **59**(7), 5072–5085, DOI: 10.1021/acs.inorgchem.0c00319.

10 S. Adhikari, O. Hussain, R. M. Phillips, W. Kaminsky and M. R. Kollipara, Neutral and cationic half-sandwich arene d6 metal complexes containing pyridyl and pyrimidyl thiourea ligands with interesting bonding modes: Synthesis, structural and anti-cancer studies, *Appl. Organomet. Chem.*, 2018, **32**(9), e4476, DOI: 10.1002/aoc.4476.

11 L. Wang, L. Liu, C. Zhang, G. Yu, W. Lin, X. Duan, Y. Xiong, G. Jiang, J. Wang and X. Liao, Design, synthesis, anti-infective potency and mechanism study of novel Ru-based complexes containing substituted adamantane as antibacterial agents, *Eur. J. Med. Chem.*, 2024, **270**, 116378, DOI: 10.1016/j.ejmech.2024.116378.

12 E. V. Suslov, E. S. Mozhaytsev, D. V. Korchagina, N. I. Bormotov, O. I. Yarovaya, K. P. Volcho, O. A. Serova, A. P. Agafonov, R. A. Maksyutov, L. N. Shishkina, *et al.*, New chemical agents based on adamantane–monoterpene conjugates against orthopoxvirus infections, *RSC Med. Chem.*, 2020, **11**(10), 1185–1195, DOI: 10.1039/D0MD00108B.

13 N. Y. Kuznetsov, R. M. Tikhov, I. A. Godovikov, M. G. Medvedev, K. A. Lyssenko, E. I. Burtseva, E. S. Kirillova and Y. N. Bubnov, Stereoselective synthesis of novel adamantane derivatives with high potency against rimantadine-resistant influenza A virus strains, *Org. Biomol. Chem.*, 2017, **15**(15), 3152–3157, DOI: 10.1039/C7OB00331E.

14 M. Li, H. Wang, D. L. Hill, S. Stinson, K. Veley, I. Grossi, J. Peggins, J. M. Covey and R. Zhang, Preclinical pharmacology of the novel antitumor agent adaphostin, a tyrphostin analog that inhibits bcr/abl, *Cancer Chemother. Pharmacol.*, 2006, **57**(5), 607–614, DOI: 10.1007/s00280-005-0094-4.

15 N. Orsolic, M. Golemovic, A. Quintás-Cardama, B. Scappini, T. Manshouri, J. Chandra, I. Basic, F. Giles, H. Kantarjian and S. Verstovsek, Adaphostin has significant and selective activity against chronic and acute myeloid leukemia cells, *Cancer Sci.*, 2006, **97**(9), 952–960, DOI: 10.1111/j.1349-7006.2006.00269.x.

16 M. E. Kukushkin, D. A. Skvortsov, M. A. Kalinina, V. A. Tafeenko, V. A. Burmistrov, G. M. Butov, N. V. Zyk, A. G. Majouga and E. K. Beloglazkina, Synthesis and cytotoxicity of oxindoles dispiro derivatives with thiohydantoin and adamantane fragments, *Phosphorus, Sulfur Silicon Relat. Elem.*, 2020, **195**(7), 544–555, DOI: 10.1080/10426507.2020.1723590.

17 M. P. Kumar, A. S. Annie, J. N. Solanke, R. Dandela and V. Dhayalan, A Comprehensive Review on Selective Catalytic Methods for Functionalization of Adamantane Scaffolds, *Asian J. Org. Chem.*, 2024, **13**(8), e202400184, DOI: 10.1002/ajoc.202400184.

18 T. H. Maugh, Panel Urges Wide Use of Antiviral Drug: NIH group says amantadine should be used for both prevention and therapy of influenza A in the next epidemic, *Science*, 1979, **206**(4422), 1058–1060, DOI: 10.1126/science.386515.

19 E. T. Warda, M. B. El-Ashmawy, E.-S. E. Habib, M. S. M. Abdelbaky, S. Garcia-Granda, S. Thamotharan and A. A. El-Emam, Synthesis and in vitro antibacterial, antifungal, anti-proliferative activities of novel adamantane-containing thiazole compounds, *Sci. Rep.*, 2022, **12**(1), 21058, DOI: 10.1038/s41598-022-25390-0.

20 Y. Zhou, K. A. Gammeltoft, A. Galli, A. Offersgaard, U. Fahnøe, S. Ramirez, J. Bukh and J. M. Gottwein, Efficacy of Ion-Channel Inhibitors Amantadine, Memantine and Rimantadine for the Treatment of SARS-CoV-2 In Vitro, *Viruses*, 2021, **13**(10), 2082, DOI: 10.3390/v13102082.

21 T. A. Blanpied, R. J. Clarke and J. W. Johnson, Amantadine inhibits NMDA receptors by accelerating channel closure during channel block, *J. Neurosci.*, 2005, **25**(13), 3312–3322, DOI: 10.1523/JNEUROSCI.4262-04.2005.

22 G. Rohini, J. Haribabu, K. N. Aneesrahman, N. S. P. Bhuvanesh, K. Ramaiah, R. Karvembu and A. Sreekanth, Half-sandwich Ru(II)(η6-p-cymene) complexes bearing N-dibenzosuberenyl appended thiourea for catalytic transfer hydrogenation and in vitro anticancer activity, *Polyhedron*, 2018, **152**, 147–154, DOI: 10.1016/j.poly.2018.06.035.

23 S. Swaminathan, J. Haribabu, M. K. M. Subarkhan, D. Gayathri, N. Balakrishnan, N. Bhuvanesh, C. Echeverria and R. Karvembu, Impact of aliphatic acyl and aromatic thioamide substituents on the anticancer activity of Ru(ii)-p-cymene complexes with acylthiourea ligands—in vitro and in vivo studies, *Dalton Trans.*, 2021, **50**(44), 16311–16325, DOI: 10.1039/D1DT02611A.

24 S. Parveen, K. K. H. Tong, M. Khawar Rauf, M. Kubanik, M. A. Shaheen, T. Söhnel, S. M. F. Jamieson, M. Hanif and C. G. Hartinger, Coordination Chemistry of Organoruthenium Compounds with Benzoylthiourea Ligands and their Biological Properties, *Chem. – Asian J.*, 2019, **14**(8), 1262–1270, DOI: 10.1002/asia.201801798.

25 L. Colina-Vegas, L. Luna-Dulcey, A. M. Plutín, E. E. Castellano, M. R. Cominetti and A. A. Batista, Half sandwich Ru(ii)-acylthiourea complexes: DNA/HSA-binding,

anti-migration and cell death in a human breast tumor cell line, *Dalton Trans.*, 2017, **46**(38), 12865–12875, DOI: 10.1039/C7DT01801K.

26 J. P. Barolli, P. I. Maia, L. Colina-Vegas, J. Moreira, A. M. Plutin, R. Mocelo, V. M. Deflon, M. R. Cominetti, M. I. Camargo-Mathias and A. A. Batista, Heteroleptic tris-chelate ruthenium(II) complexes of N, N-disubstituted-N′-acylthioureas: synthesis, structural studies, cytotoxic activity and confocal microscopy studies, *Polyhedron*, 2017, **126**, 33–41.

27 S. Swaminathan, J. Haribabu, M. K. M. Subarkhan, G. Manonmani, K. Senthilkumar, N. Balakrishnan, N. Bhuvanesh, C. Echeverria and R. Karvembu, Coordination behavior of acylthiourea ligands in their Ru (II)–Benzene Complexes— Structures and anticancer activity, *Organometallics*, 2022, **41**(13), 1621–1630, DOI: 10.1021/acs.organomet.2c00127.

28 S. Adhikari, O. Hussain, R. M. Phillips, W. Kaminsky and M. R. Kollipara, Synthesis, structural and chemosensitivity studies of arene d6 metal complexes having N-phenyl-N′-(pyridyl/pyrimidyl)thiourea derivatives, *Appl. Organomet. Chem.*, 2018, **32**(6), e4362, DOI: 10.1002/aoc.4362.

29 N. A. Ravindran, R. J. Deepak, N. Bhuvanesh and R. Karvembu, Synthesis of substituted quinazolines using Ru(II)-p-cymene catalysts containing ferrocene acylthiourea ligand via acceptorless dehydrogenative coupling, *Inorg. Chem. Commun.*, 2024, **168**, 112963, DOI: 10.1016/j.inoche.2024.112963.

30 J. Pathan, D. K. Tripathi, K. M. Poluri, A. Chalana and S. Adhikari, Molecular insight into the structural and functional aspects of arene Ru(II) complexes bearing bulky thiourea ligands, *J. Inorg. Biochem.*, 2024, **257**, 112584, DOI: 10.1016/j.jinorgbio.2024.112584.

31 G. Binzet, N. Külcü, U. Flörke and H. Arslan, Synthesis and characterization of Cu(II) and Ni(II) complexes of some 4-bromo-N-(di (alkyl/aryl) carbamothioyl) benzamide derivatives, *J. Coord. Chem.*, 2009, **62**(21), 3454–3462, DOI: 10.1080/00958970903082200.

32 A. Karim, R. E. Malekshah, Y.-T. Chu and S. C. N. Hsu, Structural modulation of acylthiourea ligands in ruthenium(II) complexes with acid–base switchable monodentate and bidentate coordination, *Inorg. Chem. Commun.*, 2025, 115464, DOI: 10.1016/j.inoche.2025.115464.

33 I. L. Mawnai, S. Adhikari, W. Kaminsky and M. R. Kollipara, Synthesis of strained complexes of arene d6 metals with benzoylthiourea and their spectral studies, *J. Organomet. Chem.*, 2018, **869**, 26–36, DOI: 10.1016/j.jorganchem.2018.05.023.

34 A. Lapasam and M. R. Kollipara, A survey of crystal structures and biological activities of platinum group metal complexes containing N-acylthiourea ligands, *Phosphorus, Sulfur Silicon Relat. Elem.*, 2020, **195**(10), 779–804, DOI: 10.1080/10426507.2020.1764956.

35 D. Obradović, S. Nikolić, I. Milenković, M. Milenković, P. Jovanović, V. Savić, A. Roller, M. D. Crnogorac, T. Stanojković and S. Grgurić-Šipka, Synthesis, characterization, antimicrobial and cytotoxic activity of novel half-sandwich Ru(II) arene complexes with benzoylthiourea derivatives, *J. Inorg. Biochem.*, 2020, **210**, 111164, DOI: 10.1016/j.jinorgbio.2020.111164.

36 D. Bożejewicz, B. Ośmiałowski, M. A. Kaczorowska and K. Witt, 2, 6-Bis ((benzoyl-R) amino) pyridine (R = H, 4-Me, and 4-NMe2) derivatives for the removal of Cu(II), Ni(II), Co(II), and Zn(II) ions from aqueous solutions in classic solvent extraction and a membrane extraction, *Membranes*, 2021, **11**(4), 233, DOI: 10.3390/membranes11040233.

37 P. N. Sathishkumar, N. Raveendran, N. S. P. Bhuvanesh and R. Karvembu, Chemoselective transfer hydrogenation of nitroarenes, ketones and aldehydes using acylthiourea based Ru(II)(p-cymene) complexes as precatalysts, *J. Organomet. Chem.*, 2018, **876**, 57–65, DOI: 10.1016/j.jorganchem.2018.08.006.

38 A. Lapasam, O. Hussain, R. M. Phillips, W. Kaminsky and M. R. Kollipara, Synthesis, characterization and chemosensitivity studies of half-sandwich ruthenium, rhodium and iridium complexes containing κ1(S) and κ2(N,S) aroylthiourea ligands, *J. Organomet. Chem.*, 2019, **880**, 272–280, DOI: 10.1016/j.jorganchem.2018.11.020.

39 B. N. Cunha, L. Colina-Vegas, A. M. Plutín, R. G. Silveira, J. Honorato, K. M. Oliveira, M. R. Cominetti, A. G. Ferreira, E. E. Castellano and A. A. Batista, Hydrolysis reaction promotes changes in coordination mode of Ru(II)/acylthiourea organometallic complexes with cytotoxicity against human lung tumor cell lines, *J. Inorg. Biochem.*, 2018, **186**, 147–156, DOI: 10.1016/j.jinorgbio.2018.06.007.

40 R. Gandhaveeti, R. Konakanchi, P. Jyothi, N. S. P. Bhuvanesh and S. Anandaram, Unusual coordination mode of aroyl/acyl thiourea ligands and their π-arene ruthenium(II) piano-stool complexes: Synthesis, molecular geometry, theoretical studies and biological applications, *Appl. Organomet. Chem.*, 2019, **33**(5), e4899, DOI: 10.1002/aoc.4899.

41 K. Jeyalakshmi, J. Haribabu, N. S. P. Bhuvanesh and R. Karvembu, Half-sandwich RuCl2(η6-p-cymene) core complexes containing sulfur donor aroylthiourea ligands: DNA and protein binding, DNA cleavage and cytotoxic studies, *Dalton Trans.*, 2016, **45**(31), 12518–12531, DOI: 10.1039/C6DT01167E.

42 M. M. Sheeba, M. M. Tamizh, L. J. Farrugia, A. Endo and R. Karvembu, Chiral (η6-p-Cymene)ruthenium(II) Complexes Containing Monodentate Acylthiourea Ligands for Efficient Asymmetric Transfer Hydrogenation of Ketones, *Organometallics*, 2014, **33**(2), 540–550, DOI: 10.1021/om4010548.

43 A. Arunachalam and R. Rengan, Synthesis and Structure of Naphthoyl Thiourea-Based Binuclear Ruthenium(II) Arene Complexes: Studies on Anticancer Activity and Apoptotic Mechanism, *ChemBioChem*, 2025, **26**(10), e202500057, DOI: 10.1002/cbic.202500057.

44 C.-M. Chien, S.-H. Yang, L.-S. Chang and S.-R. Lin, Involvement of both endoplasmic reticulum-and mitochon-

dria-dependent pathways in cardiotoxin III-induced apoptosis in HL-60 cells, *Clin. Exp. Pharmacol. Physiol.*, 2008, 1059–1064, DOI: 10.1111/j.1440-1681.2008.04968.x.

45 Z.-S. Yang, T.-S. Li, Y.-S. Huang, C.-C. Chang and C.-M. Chien, Targeting the receptor binding domain and heparan sulfate binding for antiviral drug development against SARS-CoV-2 variants, *Sci. Rep.*, 2024, **14**(1), 2753, DOI: 10.1039/B508531B.

46 (*a*) CCDC 2447963: Experimental Crystal Structure Determination, 2025, DOI: 10.5517/ccdc.csd.cc2n59kq; (*b*) CCDC 2447682: Experimental Crystal Structure Determination, 2025, DOI: 10.5517/ccdc.csd.cc2n50hc; (*c*) CCDC 2447952: Experimental Crystal Structure Determination, 2025, DOI: 10.5517/ccdc.csd.cc2n596c; (*d*) CCDC 2447951: Experimental Crystal Structure Determination, 2025, DOI: 10.5517/ccdc.csd.cc2n595b.